Journal of Cleaner Production 346 (2022) 131250

Contents lists available at ScienceDirect

Journal of Cleaner Production

journal homepage: www.elsevier.com/locate/jclepro

Sodium adsorption isotherm and characterization of biochars produced from various agricultural biomass wastes

Binh Thanh Nguyen *, Gai Dai Dinh, Hao Phu Dong, Long Ba Le

Institute of Environmental Science, Engineering, and Management, Industrial University of Ho Chi Minh City, 12 Nguyen Van Bao, Go Vap District, Ho Chi Minh City, Viet Nam

ARTICLE INFO

Handling Editor: Bin Chen

Keywords:
Adsorption isotherm
Agricultural waste
Biochar characteristics
Biomass
Salt-affected water/soil
Sodium adsorption

ABSTRACT

Agricultural biomass wastes, which may pollute the environment yet are inefficiently managed worldwide, can be recycled into biochar, which is subsequently used to remediate salt-affected environments. This creates value-added or dual benefits of treating the wastes while reclaiming saline water/soil for sustainable development. Nevertheless, a lack of knowledge about the linkage between biochar characteristics and sodium adsorption capacity may restrict the wastes from being recycled. The current study aimed to examine physicochemical, nano/microstructural, and functional-group characteristics of biochar and to assess its sodium isothermal-adsorption properties. Four biochars made from rice husk (RH-BC), corn stalks (CS-BC), longan branch (LA-BC), and coconut coir (CC-BC) were used for an isothermal-adsorption experiment. Scanning Electron Microscopy (SEM), Transmission Electron Microscopy (TEM), Brauner-Emmett-Teller surface area (BET area), pore size distribution, and Fourier Transform Infrared spectroscopy (FTIR) were used to characterize biochars, which were additionally analyzed for 9 parameters. RH-BC had the highest BET area (151 $m^2\ g^{-1}$) and porosity, whereas LA-BC exhibited the lowest BET area (10.6 $m^2\ g^{-1}$), and LA-BC was more condensed. Functional groups, necessary for cation adsorption, were found in biochars. The maximum adsorption capacity of RH-BC (33.9 mg g^{-1}), estimated by the Langmuir isotherm model, was the highest while that of CC-BC (15.5 mg g^{-1}) was the lowest. The Dubinin-Radushkevich isotherm model showed that the Na adsorption mechanism was dominantly a physical process. The current study provides a feasible value-added and sustainable strategy of recycling agricultural biomass wastes with dual benefits of waste treatment and salt-affected environment remediation, applicable worldwide.

1. Introduction

Annually, global agricultural production generates a large volume of biomass waste, which is inefficiently treated and/or managed. The agricultural biomass waste may pollute the living environment, adversely influencing human health, while treating the waste may lead to significant economic loss (Isaac and Olufemi, 2020). The biomass waste can be utilized in different ways, such as a soil amendment, soil protection, biofuel production, animal feed, and other purposes, as well as on-field free burning (Sarkar et al., 2020; Isaac and Olufemi, 2020; Tripathi et al., 2019). Each way of treating agricultural biomass waste has its own set of advantages and disadvantages with varying benefits. Biomass waste can be recycled to produce biochar for a variety of applications (Haris et al., 2021; Nguyen et al., 2021; Nan et al., 2021), including salt-affected soil remediation (Gunarathne et al., 2020; Saifullah et al., 2018). Nevertheless, the effectiveness of the pathway of recycling agricultural biomass waste could be dependent on the linkage between agricultural biomass waste, biochar characteristics, and biochar's sodium adsorption capacity which is insufficiently discussed in the literature.

The rapid expansion of salt-affected regions of inland soil and freshwater bodies due to various reasons such as seawater intrusion is one of the most damaging environmental stresses, producing a considerable drop in agricultural yield and quality (Machado and Serralheiro, 2017; Shrivastava and Kumar, 2014). The salt-affected environments may include land and water bodies containing a high level of salt of sodium (Na), which greatly restricts the growth and yield of many crops (Machado and Serralheiro, 2017; Sahab et al., 2021). The salt-affected environments should be remediated for better crop productivity and the aquatic environment in order to meet global food and water demand.

* Corresponding author.
E-mail address: nguyenbinh@iuh.edu.vn (B.T. Nguyen).

https://doi.org/10.1016/j.jclepro.2022.131250
Received 4 August 2021; Received in revised form 18 December 2021; Accepted 6 March 2022
Available online 8 March 2022

As a result, removing Na from salt-affected environments is critical for sustainable development.

Sodium adsorption is one of the few important ways for reducing/removing the Na concentration of salt-affected environments (Amini et al., 2016; Minhas et al., 2020). Na adsorption on three reusable zeolites was reported by Shrivastava and Kumar (2014) with relatively low maximum adsorption capacities (from 5.6 to 11.3 mg g^{-1}). The removal of Na from saline water using amorphous carbon thin film as an adsorbent was reported by Fathy et al. (2017) with high Na adsorption capacities (107, 120, and 135 mg g^{-1}). Nonetheless, the relatively complicated production process of amorphous carbon thin film (Fathy et al., 2017) may lead to additional environmental pollution from waste acids. Biochar had been shown as a promising adsorbent with a considerable maximum adsorption capacity for removing Na from saline water (Rostamian et al., 2015). The effects of biochar on Na removal may vary, depending on its characteristics, which are determined by biomass feedstocks used to produce biochar. Nevertheless, our literature search revealed that insufficient studies have been carried out to investigate the linkage between biomass feedstocks and biochar characteristics, as well as its sodium adsorption capacity (Rostamian et al., 2015; Awan et al., 2020).

Biochar, a carbon-rich substance, can be produced from various organic carbon-based materials, such as rice husk and straw, rubberwood, coffee husk, corn stalks, and coconut biomass through the pyrolysis process (Gamage et al., 2016; Dharmakeerthi et al., 2012; Dume et al., 2015). Biochar has been studied and used in multidisciplinary areas for various purposes (Nguyen et al., 2018; Al-Wabel et al., 2017; Kaur and Sharma, 2020). Biochar is also an effective adsorbent of various organic and inorganic contaminants in the environment (Bispo et al., 2018; Zhang et al., 2021) with a few primary mechanisms including (1) electrostatic interactions, (2) cation exchange; (3) complexation with functional groups; (4) precipitation to form insoluble compounds; and (5) reduction and subsequent sorption of the reduced metal species (Li et al., 2017). Its adsorption capacity is highly greatly dependent on biochar characteristics such as surface area, pore size distribution, and ion-exchange capacity, mineral composition, and surface functional groups (Li et al., 2017; Saeed et al., 2021), which greatly vary with feedstocks (Li et al., 2017; Ahmad et al., 2013). Some feedstocks such as rice husk, corn stalks, longan branch, and coconut coir, considered as agricultural biomass wastes, are widely available in many countries throughout the world. Using these widely available feedstocks to produce biochar, which is then used for Na adsorption, is a value-added and multi-benefit solution for controlling environmental pollution caused by agricultural biomass wastes. This could be done by recycling the wastes and reclaiming salt-affected environments through biochar's adsorption capacity.

However, our most recent search revealed that, while many studies have been conducted to examine the biochar's capacity to adsorb organic and organic contaminants (Ambaye et al., 2020; Ahmad et al., 2013; Betts et al., 2013), only a few studies were conducted to examine its adsorption capacity of sodium. Therefore, the current study was carried out on four biochars made from agricultural biomass wastes for Na adsorption. The current study aimed to (1) investigate the physico-chemical, nano/micro-structural, and functional-groups characteristics of biochars and (2) assess their sodium isothermal-adsorption properties. We hypothesize that biochar produced from non-wood stem crops such as rice husk and corn stalk adsorbed more Na than biochar from the wood-stem tree, such as longan tree and that the adsorption mechanism is mainly a physical process.

2. Materials and methods

2.1. Experimental materials

Four biochars were produced from agricultural biomass wastes, which were rice (*Oryza sativa*) husk, corn (*Zea mays* L.) stalks, longan (*Dimocarpus longan Lour.*) branches, and coconut (*Cocos Nucifera* L.) coir. More details about these biomass wastes were shown in Text S1 (Supplemental Material). The pyrolysis temperature of around 350 °C was used to produce biochars because this relatively low biochar-producing temperature was found/estimated to have greater economic efficiency and chemical functional groups of the generated biochars **(Li *et al.*, 2017)** for sodium adsorption. The formed biochars were labeled as RH-BC (rice-husk biochar), CS-BC (corn-stalk biochar), LA-BC (longan biochar), and CC-BC (coconut-coir biochar). Some adsorption-related characteristics of these biochars are shown in Table 1, Figs. 1–4.

The experimental salt solutions were made by dissolving pure salt of sodium chloride in distilled water at six concentrations of 0, 0.25, 0.5, 1.0, 2.0, and 3.5 (%), which were equal to 0, 1438, 2875, 5750, 11,500, and 20,125 (mg L^{-1} Na^{+}), respectively. The salt concentrations used in the current study were selected because the highest concentration of 3.5 (%) salt was similar to that of the seawater (Schnepf et al., 2014), while the others fell within thresholds by Richards (1954) for classifying soil salinity. These experimental solutions were made and used for the adsorption experiment immediately.

2.2. The experiment of sodium isothermal adsorption

The isothermal adsorption experiment was carried out by weighing 1.5 g of each biochar into a 50-mL **centrifuge tube containing a 30-mL salt solution of varying Na concentrations (0, 0.25, 0.5, 1.0, 2.0, and 3.5%).** The experimental tubes were shaken on an end-over-end shaker for 24 h before being allowed to settle for 1 h at room temperature. The supernatant from the experimental tubes was filtered using Whatman filter paper into centrifuge tubes and the filtrate in the tubes was acidified by adding 3 drops of HNO_3 and kept in a 4 - ^{o}C refrigerator until measurement. The adsorption experiment was conducted in four replicates and a total of 96 experimental tubes (4 (biochars) x 6 (experimental salt solutions) x 4 (replicates)) were created for the experiment.

2.3. Measurements

Six raw biochars were ground till they passed through a 2-mm sieve before being measured for pH, EC, Na, K, Ca, Mg, Al, Fe, Mn, organic C, and ash content. The material was mixed with distilled water at a 1:5 (w/w) ratio and the extract was measured for pH and EC using a pH meter and an EC meter, respectively. The concentration of exchangeable Na, K, Ca, Mg, Al, Fe, and Mn was determined using the barium chloride method (Carter and Gregorich, 2008), and the extract was measured using an Inductively coupled plasma-optical emission spectrometry (ICP-OES). The ash content was determined by heating 2 g of individual biochars overnight at 600 °C. All of these measurements were carried out in four replicates. The 96 acidified filtrates after the experiment were analyzed for Na, K, Ca, and Mg using an ICP-OES.

The micro-scale morphology of the four biochars was characterized using a scanning electron microscope (SEM, model LE01430VP, Germany). The Brunauer-Emmett-Teller surface area (BET area) and pore size distribution of the four biochars were determined using a NOVA 4000E Brunauer - Emmett - Teller Surface Area and Pore Size Analyzer (Quantachrome Instruments) using nitrogen adsorption isotherms at 77.3 K. The porosity of the four biochars was estimated from the SEM image using ImageJ program (Astuti et al., 2018). The nano-scale structure of four biochars was captured using a high-resolution transmission electron microscope (JEM 2100, JEOL). Fourier Transform Infrared (FTIR) analysis was applied on four biochars to examine their functional groups using the method developed by Li et al. (2020) on a Jasco FT/IR-4700 type A spectrophotometer. The wavenumber associated with spectral peaks of individual functional groups was determined, based on (Kaur et al., 2020), (Daffalla et al., 2020), and (Mireles et al., 2019). Raman spectroscopy of the four biochars was carried out using a Raman spectrometer (Raman Horiba Zplora plus Raman

Table 1
Selected physicochemical properties of the four biochars. n = 4.

Biochars	EC	pH	Ash content	Na	K	Ca	Mg	Al	Fe	Mn
	(dS m^{-1})		(%)	(mg g^{-1})						
Mean										
RH-BC	0.31	8.5	49.19	2.28	10.88	2.86	0.50	0.010	0.028	0.014
CS-BC	5.15	9.1	21.54	3.70	80.75	7.21	1.08	0.016	0.207	0.036
LA-BC	0.19	7.2	4.76	1.38	0.97	3.12	0.28	0.006	0.002	0.016
CC-BC	3.64	9.4	12.49	23.85	64.34	2.74	1.11	0.104	0.165	0.014
Standard error										
RH-BC	0.004	0.05	0.44	0.080	0.114	0.220	0.024	0.0003	0.0003	0.0011
CS-BC	0.026	0.08	0.08	0.238	1.900	0.449	0.083	0.0010	0.0049	0.0022
LA-BC	0.014	0.05	0.82	0.099	0.029	0.229	0.013	0.0004	0.0001	0.0011
CC-BC	0.022	0.05	0.18	0.529	1.956	0.379	0.080	0.0023	0.0050	0.0019

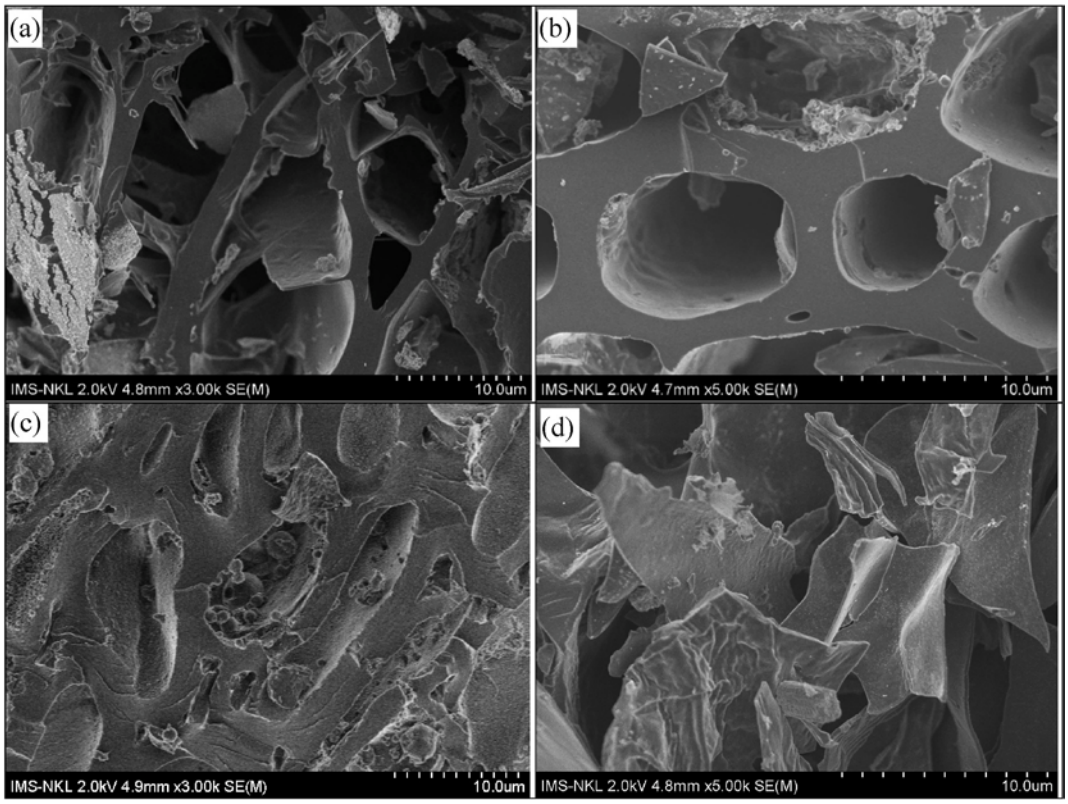

Fig. 1. Micro-scale morphology of biochars produced from rice husk (a), corn stalks (b), longan branch (c), and coconut coir (d) captured by using a Scanning Electron Microscopy (SEM).

microprobe, France) with a laser 532 nm as a laser excitation, the power of 3.2 mW, and acquisition time of 10 s for one measurement (Pham et al., 2021). Peak fitting of Raman spectra to proximately estimate the carbonaceous structure of the associated biochars was conducted based on the method by **(Sousa *et al.*, 2020; Maliutina *et al.*, 2018)** and using Originpro 2018 (OriginLab Corporation, Northampton, Massachusetts, USA). Raman shifts at 1586, 1362, 1683, 1501, and 1174 cm^{-1} were assigned to bands of G, D1, D2, D3, and D4, respectively (Maliutina et al., 2018).

2.4. Modeling and statistical analyses

The Langmuir isotherm model (LMM) and the Dubinin-Radushkevick isotherm model (DRM) were used to examine the dependency of the adsorbed quantity of Na on the Na concentration at equilibrium, thereby estimating the maximum adsorption capacity and adsorption mechanism of Na on biochars. More details of these two models were shown in Text S2 (Supplemental Material). In addition, Analysis of Variance (ANOVA) as a completely randomized design with four replicates was conducted to examine the difference between the biochars. The exponential functions were also fitted to examine the relationships between the adsorbed quantity of Na at equilibrium and the salt concentration of the experimental solution. All figures and model fittings were carried out using Sigmaplot 12 (Systat Software Inc.).

3. Results

3.1. Chemical properties of biochars

The chemical properties of the four biochars used in the current study were shown in Table 1. The RH-BC contained the highest ash content of around 49.19 (%) of the total mass. The CS-BC had the greatest values of EC, pH, and the concentration of exchangeable K, Ca, Al, Fe, and Mn. It was important to notice that the CC-BC had the

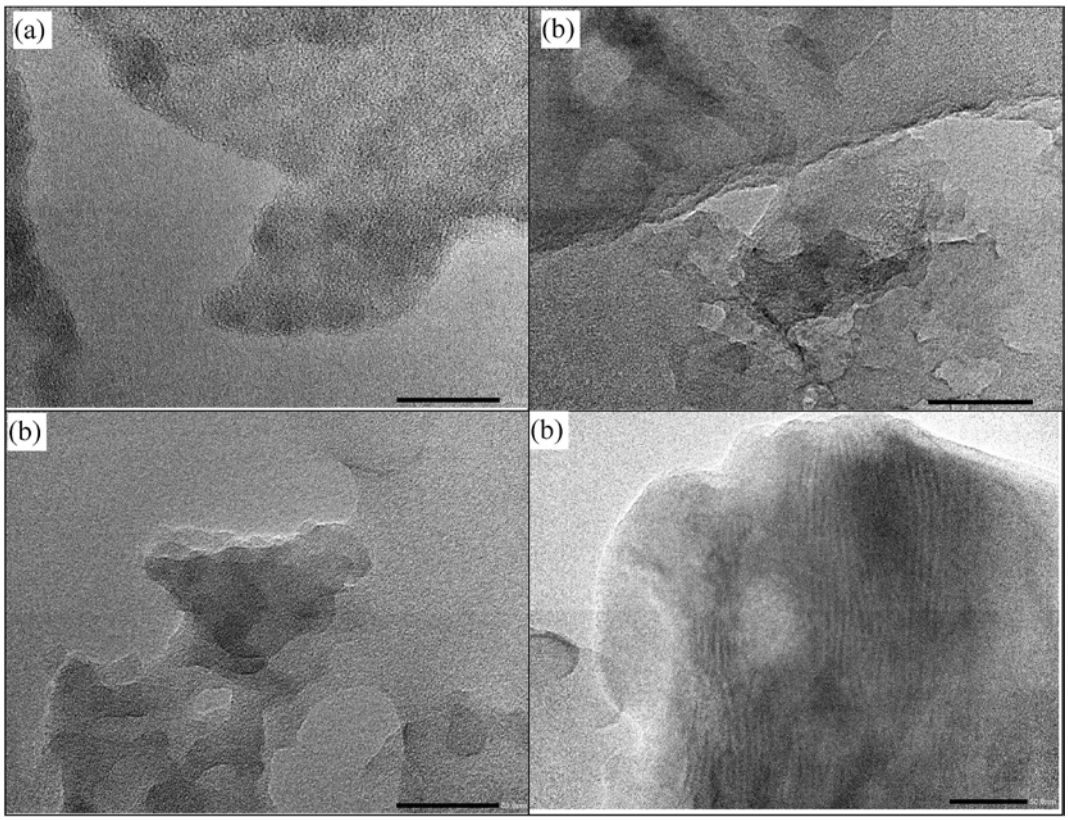

Fig. 2. Nanoscale structure of the tested biochars produced from rice husk (a), corn stalks (b), longan branches (c), and coconut coir (d) captured using a Transmission Electron Microscopy (TEM).

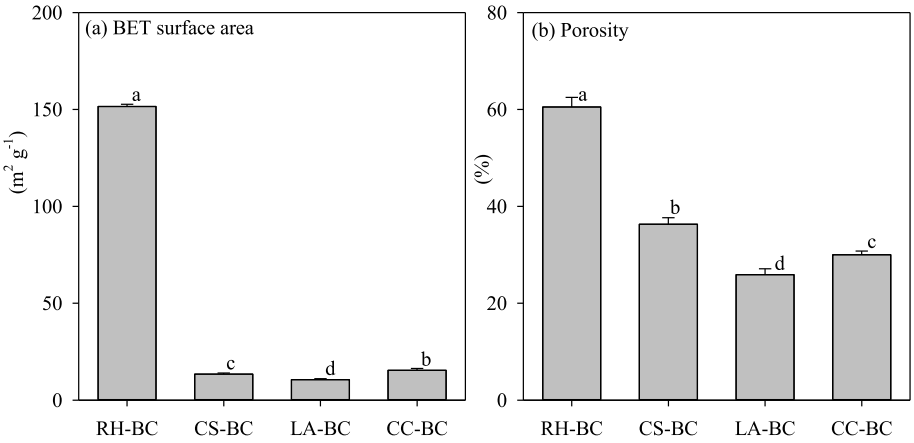

Fig. 3. The BET surface area (a) and porosity (b) of four biochars. Notice the porosity was estimated, using ImageJ software. Within a panel, bars attached with the same letter were not significantly different.

greatest concentration of exchangeable Na (23.83 mg g^{-1}), compared to the other biochars varying from 1.38 to 3.70 (mg g^{-1}). The LA-BC had the lowest values of EC, pH, and the concentration of exchangeable Na, K, Mg, Al, Fe, and Mn.

3.2. Micro- and nano-structure of biochars

Fig. 1 showed that biochar made from rice husk had more micro-size pores than the other biochars, and biochar produced from longan had fewer pores than those produced from rice husk and corn stalks. Biochar made from coconut coir exhibited limited microstructural pores and its image showed various small fragments. TEM images at the nanoscale of the four biochars were shown in Fig. 2. Biochars were composed of short C layers of amorphous structure with no lattice structure. Carbon layers of the LA-BC were stacked over each other, making this biochar more condensed than the other biochars. Some fiber-liked shape of the C layer was seen from the TEM image of the CC-BC.

3.3. BET area, and pore size distribution

The surface area of the RH-BC was significantly highest, around 151 (m^2 g^{-1}), followed by CC-BC (15.4), CS-BC (13.4), and LA-BC (10.6, m^2 g^{-1}) (Fig. 3a). Similarly, the porosity (Fig. 3b) of the RH-BC was the highest (around 60.5%), and that of the LA-BC was the lowest (around

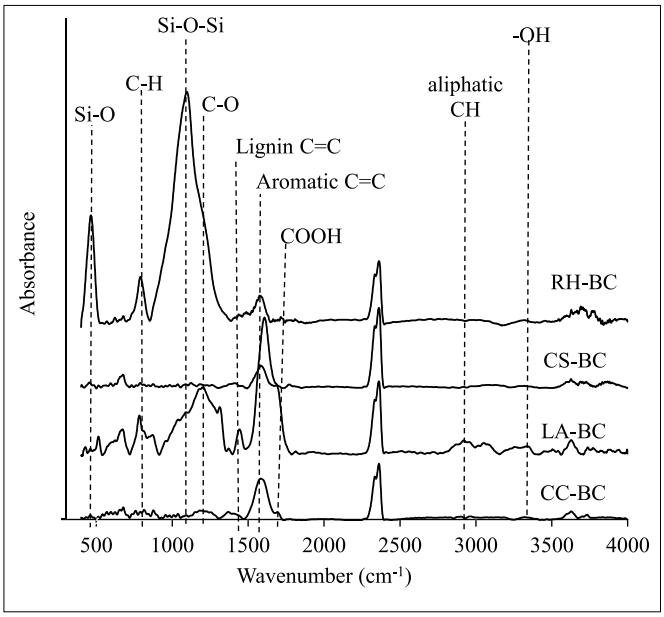

Fig. 4. Fourier-transform infrared (FTIR) spectra of the four biochars used for the current study.

25.9% of the total cross-section image area shown in Fig. 1. The total pore volume of the RH-BC was the highest, followed by CC-BC, CS-BC, and LA-BC (Fig. S1, Supplemental Material). The RH-BC had the highest pore volume at pore diameter rank from 1 to 5 nm; the CS-BC was from 1.5 to 4.5; the LA-BC was from 2 to 5, and CC-BC was from 1.5 to 5 nm (Fig. S1, Supplemental Material).

3.4. Fourier-transform infrared (FTIR) and Raman spectroscopy

The FTIR spectra (Fig. 4) showed that the biochars contained vibrational peaks at 3404.3, 2862–2921, 1641.3–1737.7, 1546.8–1652.9, 1440–1510, 1153.4–1300, 1080, 780–800, and 451-467 cm^{-1}, which were associated with functional groups of O–H, aliphatic C–H, COOH, aromatic C = C, lignin C═C, C–O, Si–O–Si, C–H, and Si–O, respectively. RH-BC had the largest amount of Si element with peaks at 1080 and 476 cm^{-1}, while the other biochar did not have strong peaks at these wavenumbers. All four biochars exhibited a strong peak at 1546.8–1652.9 cm^{-1} of the aromatic C═C group. The LA-BC had a high peak at 1153.4–1300 cm^{-1}, which could be from the C–O stretching of aromatic ester or aliphatic ether. The RH-BC and LA-BC had a strong peak at 780-800 cm^{-1}, which could be derived from the C–H bending. Raman spectra and their peak fitting of the four biochars were shown in Fig. S2 (Supplementary material). The spectra had two dominant peaks at around 1362 and 1586 (cm^{-1}), which were designated as D and G bands. The intensity and bandwidth of G, D1, D2, D3, and D4 varied greatly with biochars. The bandwidth of the D4 band of RH-BC, CS-BC, and CC-BC and that of the D2 band of LA-BC was broader than that of the D1 and G bands.

3.5. Adsorption and desorption of Na, K, Ca, and Mg

The amount of Na adsorbed on biochars was significantly increased exponentially with an increase in the salt concentration of the experimental salt solution, (Fig. S3, Supplemental Material). Na was released from all four biochars into the experimental zero-salt solution, as shown by negative values of the adsorbed Na. The lowest negative value (−19.5 mg g^{-1}), indicating the desorption of Na, was observed on the CC-BC. For the experimental solutions with salt concentrations ranging from zero to around 1 (%), the Na quantity adsorbed was increased rapidly and leveled off afterward. The RH-BC adsorbed the most Na, followed by the CS-BC, LA-BC, and CC-BC.

Biochars also released a certain quantity of cations, such as K, Ca, and Mg into the experimental solution, depending on biochars and the salt content of the experimental solution (Table S1, Supplemental Material). In general, an increase in salt concentration in the experimental solution resulted in an enhanced quantity of these cations released from the four biochars. The released quantity of K, Ca, and Mg from RH-BC was significantly increased, whereas that from CC-BC was slightly similar across the six salt concentrations.

3.6. Adsorption isotherm of sodium on biochars

The Langmuir isotherm model (LMM) and Dubinin-Radushkevich isotherm model (DRM) were both appropriate for examining the adsorption isotherm of Na with coefficients of determination (r^2) greater than 95 (%) (Table S2, Supplemental Material). Fig. 5a showed that the maximum adsorption capacity for Na of RH-BC was significantly the highest, around 33.9, followed by CS-BC (30.9), LA-BC (17.9, and CC-BC (15.5 mg g^{-1}). The free adsorption energy of the RH-BC estimated by the DRM was also the highest, whereas that of the CC-BC was the lowest. The adsorption energy of the four biochars was less than a threshold of 8 (kJ mol^{-1}) (Fig. 5b), indicating that Na adsorption on the four biochars was mainly a physical process.

3.7. The exchange ratio

The exchange ratio of the adsorbed Na to the total of released K, Ca, and Mg was calculated and shown in Fig. 6. In general, an increase in salt concentration in the experimental solution resulted in an enhanced ratio from negative values to about 6, depending on biochars. The ratio was negative for the zero-salt solution due to Na desorption from biochars. Two biochars, RH-BC and LA-BC, exhibited the highest ratio at salt concentrations ranging from 1 to 2 (%), but a further increase in the salt concentration led to a reduced ratio. For the other two biochars, CS-BC and CC-BC, the ratio was rapidly raised from zero to around 1 (%)-salt concentration and then leveled off.

4. Discussion

4.1. Adsorption–related characteristics of biochars

Of the four biochars tested in the current study, the CC-BC had the highest content of exchangeable Na, 23.83 (mg g^{-1}), which can be discharged into the experimental solution, accounting for the lowest negative value of Na at the zero-salt concentration (Fig. S3, Supplemental Material). Coconut coir contained a high concentration of Na, K, and Cl (Xiong et al., 2017), responsible for a very high concentration of Na (23.85) and K (64.34 mg g^{-1}) of the biochar made from the coconut coir. In Vietnam, the coconut tree is grown in salt-affected soils, which may result in its biomass being rich in salt elements such as Na. The LA-BC, on the other hand, contained the lowest concentration of exchangeable Na (1.38 mg g^{-1}). In comparison to the other biomass wastes used to make biochars in the current study, the longan branch as hardwood had a higher density and was more condensed which could be observed from the microscale SEM images in Fig. 1. Additionally, the lowest ash content of the LA-BC (Table 1) may account for the lowest concentration of the exchangeable Na, K, Mg, and Fe of this material. The highest ash level of the RH-BC could be attributed to the great Si concentration contained in the material (Wang et al., 2018; Do et al., 2019). The high Si content of the RH-BC could be also inferred from the FTIR spectra (Fig. 4), which revealed two great peaks at 1080 and 476 cm^{-1} for this material.

The great difference in the four biochars can be seen through SEM micro-scale morphology (Fig. 1), TEM nano-scale image (Fig. 2), BET surface area, porosity (Fig. 3), and pore size distribution (Fig. S1, Supplemental Material). Pyrolysis temperature raised the BET surface area

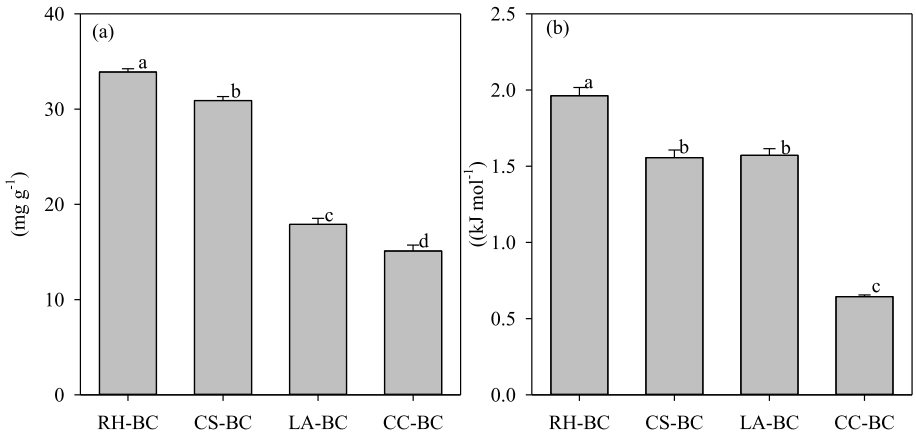

Fig. 5. Maximum adsorption capacity (a) based on the LMM and free adsorption energy (c) based on the DRM of four biochars. Within a panel, bars attached with the same letter were not significantly different at $P < 0.05$. The error bars indicated standard error. $n = 4$.

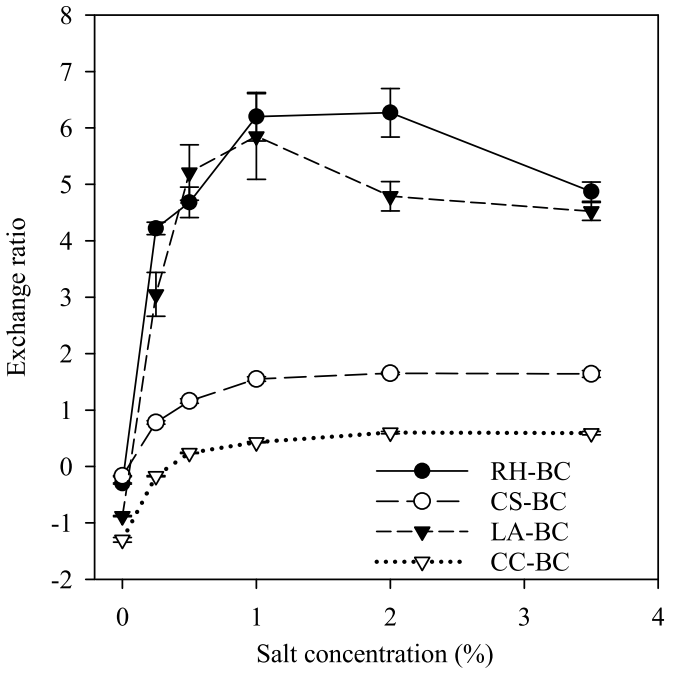

Fig. 6. Exchange ratio (adsorbed Na to the sum of released K, Ca, and Mg) of four biochars over the tested salt concentrations.

of biochars by destructing labile organic carbon substances and certain functional groups such as aliphatic alkyls and ester groups, exposing the aromatic lignin core (Tomczyk et al., 2020; Leng et al., 2021). The low BET surface areas of the CS-BC (13.4), LA-BC (10.6), and CC-BC ($m^2\ g^{-1}$) were within the lowest range documented by Leng et al. (2021). For a temperature range below 600 °C, an increase in pyrolysis temperature would enhance the BET surface area of biochar (Leng et al., 2021). The pyrolysis temperature applied in the current study was around 350 °C, which more likely resulted in the biochars having the lowest BET surface area. The BET surface area and porosity of biochars can be primarily determined by two factors of biomass feedstock and the pyrolysis method (Leng et al., 2021). While the latter applied to produce the four biochars in the current study was the same, the former was different. Tomczyk et al. (2020) reported that the low surface area accompanied by a low ash content (determined by feedstock) was found from some biochars produced from cottonseed hull, poultry litter, and dairy manures. Similarly, the current study found that the RH-BC contained the greater ash content and the BET surface area, whereas the LA-BC had the lowest ash content as well as BET surface area. The difference in the BET surface area and porosity of the four tested biochars could be attributed to the physical structure of the biochar-producing biomass wastes (paddy rice and corn are cereal grass crops with non-wood stem, while the longan is a hardwood stem tree and coconut coir is a natural fiber). Fewer structural pores of the CC-BC (Fig. 1d) may result in the lower porosity of the material, relative to the RH-BC and CS-BC (Fig. 3). Additionally, the micro-scale morphology of the four biochars (Fig. 1) may suggest that LA-BC was more condensed than the other biochars, leading to the lowest BET surface area and porosity of this material. The TEM image (Fig. 2) also showed that the nano-structure of C layers of the four biochar was mainly amorphous, rather than any well-organized arrangement, such as graphite. Furthermore, Fig. S2 (Supplementary material) revealed that the defect D4 band (RH-BC, CS-BC, and CC-BC) and defect D2 band (LA-BC) from Raman spectra had a wider bandwidth than the D1 and G bands, respectively, indicating that the carbon structure of the four biochars was highly amorphous (Maliutina et al., 2018). The amorphous structure, presumably as a result of low pyrolysis temperature, may lead to greater adsorption of inorganic pollutants because of the presence of more oxygen-functional groups (Hassan et al., 2020).

Biochar could contain important multiple functional groups (Chen et al., 2015), which are required for cation adsorption. The FTIR spectra of the four biochars showed eight peaks, which varied, depending on biochar-produced agricultural wastes. The RH-BC, for example, displayed great peaks at 1080 and 451-467 cm^{-1}, which were assigned to asymmetric Si–O–Si stretching and Si–O bending vibration, respectively (Wang et al., 2019), indicating that the material contained a high Si content. The surface functional groups may remove cations from the surrounding environment through various mechanisms associated with oxygen-containing functional groups on the adsorbent's surface (Mireles et al., 2019; Ahmad et al., 2013; Guo et al., 2020). Some cation adsorption-related functional groups identified from the biochar's spectra in the current study (Fig. 4) may include amine (C–N) and/or aromatic ester and alkyl aryl ether (C–O at 1153.4–1300 cm^{-1}), carboxyl (COOH at 1641.3–1737.7), hydroxyl (OH at 3404.3), aliphatic CH (at 2862–2921), (Mireles et al., 2019; Deliyanni et al., 2012; Guo et al., 2020). All four biochars containing these functional groups in varying proportions indicated that the tested materials can be potential adsorbents for ionic Na in salt-affected environments.

4.2. Biochar as a sodium adsorbent

The maximum adsorption capacity of sodium on the four tested biochars in the current study was determined using the LMM, which fitted the Na adsorption data well ($r^2 > 0.95$) (Table S2, Supplemental

Material). Many studies used the LMM to estimate the adsorption capacity of cations, including Na, on biochar with a high coefficient of determination (Awan et al., 2020; Wu et al., 2019; Mireles et al., 2019; Fidel et al., 2018). These indicate that the Na adsorption on biochar surface could be considered as a homogeneous monolayer, based on the hypothesis for the LMM (Hettiarachchi et al., 2015).

Fig. 5b showed that the RH-BC adsorbed the most Na, followed by CS-BC, LA-BC, and CC-BC. Many factors, including surface area, porosity, pore size distribution, and functional groups, can collectively determine Na adsorption, which was primarily a surface phenomenon (Chatterjee et al., 2020; Li et al., 2017; Rostamian et al., 2015). The surface area and porosity could be the most important features for adsorption in providing adsorption sites and space for adsorbates to be adsorbed because adsorption is known as a process of accumulating the adsorbate on the adsorbent's surface. The BET surface area (151.5 m^2 g^{-1}) and porosity (60.5%) of the RH-BC much greater than those of the other biochars (Fig. 3) could be likely the main reason to explain the greatest adsorption capacity of the RH-BC, relative to the other biochars. Similarly, Saeed et al. (2021) showed a strong positive relationship between surface area and Cd^{2+} adsorption capacity on activated biochar. The cadmium (II) adsorption capacity was strongly dependent on the enhanced surface area of biochar as an adsorbent produced from different raw materials and pyrolysis temperatures (Chen et al., 2014). The lowest pore size of RH-BC was from around 1 nm; that of CS-BC was from around 1.5 nm, LA-BC from around 2, and CC-BC from around 1.5 nm (Fig. S1, Supplemental Material). Meanwhile, sodium has an ionic radius of 0.102 nm and a hydrated radius of 0.358 nm (Cheng et al., 2018), indicating that its size (ionic and hydrated diameters) was well smaller than the smallest pore diameter of the four biochars. This may imply that ionic Na could easily penetrate the nanopores of the biochars for surface adsorption and so the pore size distribution of four biochars in the current study may play a minor role in determining the adsorption capacity.

Several studies were conducted to quantify the adsorption capacity of Na on biochar. For example, the maximum adsorption capacity of Na on rice-husk biochar was reported to vary from 35.2 to 53.9 (mg g^{-1}) (Rostamian et al., 2015), depending on pyrolysis temperature. The current study showed that the maximum adsorption capacity of Na on rice-husk biochar was around 33.9 (mg g^{-1}). The low pyrolysis temperature (around 350 °C) could be the reason to explain the adsorption capacity of Na on rice-husk biochar from the current study lower than those reported by Rostamian et al. (2015). Meanwhile, Awan et al. (2020) reported that biochar produced from hemp can adsorb Na up to 0.923 (mg g^{-1}), which is much low than the results of the current study. The sodium adsorption capacity of a **mixture of hardwood and softwood produced at 500 °C was reported to be about** 60 (mg g^{-1}) **(Akhtar *et al.*, 2015), which was well greater than those found from the current study**.

4.3. Adsorption mechanisms

The current study used the DRM (Dubinin-Radushkevich isotherm model) to primarily investigate the process of Na adsorption (Ayawei et al., 2017) on the tested biochars. The results from Table S2 (Supplemental Material) indicated that DRM was appropriately applied with high coefficients of determination (more than 0.95). The Gibbs free energy for Na adsorption on biochar was lower than 8 (kJ mol^{-1}), indicating that Na adsorption was predominantly a physical process (Taha et al., 2017). The process may include hydrogen bonding, van der Waals forces, electrostatic forces, hydrophobic interactions, and electrostatic interactions (Zhang et al., 2016; Awan et al., 2020). The preceding explanation revealed the tested biochars in the current study may adsorb Na through their functional groups such as OH, COOH, CH, especially CO/CN (Fig. 4) (Mireles et al., 2019; Guo et al., 2020). The chemical functional groups of biochars identified in the current study could physically interact with ionic Na to retain it on the biochar's surface, forming the physical process of adsorption.

Additionally, biochars released a certain quantity of Na (clearly observed at the zero-salt concentration, Fig. S3, Supplemental Material) and other cations such as K, Ca, and Mg (observed at all salt concentrations, Table S1, Supplemental Material). Biochars used in the current study were made from agricultural biomass wastes (rice husk, corn stalks, longan branch, and coconut coir), which contained a certain quantity of these elements. Similarly, Awan et al. (2020) observed that some elements such as Ca, Mg, and Na were released to the extracted solution from their tested biochars. High Na concentration in the experimental solution increased concentrations of K, Ca, and Mg in the experimental solution after the adsorption experiment, suggesting that an ion-exchange mechanism may exist in the current study. The exchange ratio of the CC-BC was less than 1 at all six salt concentrations (Fig. 6), implying that the quantity of Na adsorbed was less than the quantity of K, Ca, and Mg released into the solution. The exchange ratio of the CS-BC varied around the number 1, when the salt concentration changed from 0.25 to 3.5 (%), suggesting that the adsorbed Na was relatively equal to the total of K, Ca, and Mg released. The two other biochars (RH-BC and LA-BC) had a similar exchange ratio, which reached the highest value at the salt concentration of around 1 (%). The exchange ratio of the two biochars was much higher than 1 for the salt concentrations above 0.25 (%), indicating that these biochars adsorbed a greater quantity of Na while releasing a relatively lower amount of K, Ca, and Mg.

These findings suggest that biochars made from agricultural biomass wastes at low pyrolysis temperatures (350 °C) can retain a certain quantity of Na from the environment. Two mechanisms responsible for the adsorption may include the physical adsorption and ion exchange process. This indicates that biochars also release a certain quantity of some cations such as Na, K, Mg, and Ca, which are contained in the biomass wastes. The released cations may increase the salinity and Na concentration of the salt-affected environments which requires additional attention in reclamation. Washing out cations contained in biochars before their application could be an option for reducing the feedback effects of the released cations. On the other hand, the selection of agricultural biomass waste for biochar production, such as rice husk and its biochar, should be the most important in remediating the salt-affected environments to archive the greatest effect for sustainable development.

5. Conclusions and implication

The results from the current study demonstrated that the sodium adsorption capacity was strongly linked to biochars' characteristics, which were determined by agricultural biomass wastes. Of the four tested biochars, the rice-husk biochar with the greatest BET surface area (151 m^2 g^{-1}) and porosity (60.5%) exhibited the highest adsorption capacity of sodium (33.9 mg g^{-1}). Other biochars made from corn stalks, longan, and coconut coir had significantly lower BET surface area varying from 10.6 to 15.4 (m^2 g^{-1}), and sodium adsorption capacity ranging from 15.5 to 30.9 (mg g^{-1}). Biochar derived from corn stalks exhibited a lower BET surface area (13.4 m^2 g^{-1}) but higher sodium adsorption capacity (30.9 mg g^{-1}) than biochar derived from coconut coir (15.4 m^2 g^{-1} and 15.1 mg g^{-1}, respectively), which could be attributed to differences in chemical functional groups and porosity of the tested biochars. The micro and nanoscale images of the biochars help explain the difference in porosity, BET surface area, and consequent sodium adsorption capacity of the biochars. The Na adsorption mechanism was dominantly a physical process and the ion-exchange mechanism also played an important role. In brief, the analyses of the physical, chemical, morphological, nano-structural, and chemically functional-group properties, as well as Na adsorption experiment on the four biochars, strongly confirmed that the rice-husk biochar is a potential adsorbent and the coconut-coir biochar is a poor adsorbent to remove ionic Na from the salt-affected environments. These findings indicate

that recycling agricultural biomass wastes, such as rice husk, into biochar, which is subsequently used to reclaim salt-affected environment, is a sustainable management strategy. It creates additional value to the treatment of agricultural biomass wastes. This strategy offers dual benefits of treating agricultural biomass wastes while reclaiming salt-affected water/soil, which can be applied worldwide for sustainable development.

Conflict of interest

The authors have no conflict of interest to declare.

CRediT authorship contribution statement

Binh Thanh Nguyen: Conceptualization, Methodology, Writing – original draft, Writing – review & editing, Funding acquisition. **Gai Dai Dinh:** Writing – original draft, preparation. **Hao Phu Dong:** Methodology, Investigation, Resources. **Long Ba Le:** Supervision, Formal analysis, Methodology.

Declaration of competing interest

The authors declare that they have no known competing financial interests or personal relationships that could have appeared to influence the work reported in this paper.

Acknowledgments

This work was financially supported by the Foundation of Science and Technology Development of Ho Chi Minh City (HCM-FOSTED), under contract No. 36/2020/HĐ-QPTKHCN, signed on July 13, 2020. The authors are grateful to the Industrial University of Ho Chi Minh City (IUH) and the Institute of Environmental Science, Engineering, and Management (IESEM) of IUH. Many thanks are given to the staff and students at IESEM for their help with field trips and lab experiments.

Appendix A. Supplementary data

Supplementary data to this article can be found online at https://doi.org/10.1016/j.jclepro.2022.131250.

.

References

Ahmad, M., Rajapaksha, A., Lim, J.E., Zhang, M., Bolan, N., Mohan, D., Vithanage, M., Lee, S.S., Ok, Y.S., 2013. Biochar as a sorbent for contaminant management in soil and water: a review. Chemosphere 99. https://doi.org/10.1016/j.chemosphere.2013.10.071.

Akhtar, S.S., Andersen, M.N., Liu, F., 2015. Biochar mitigates salinity stress in potato. J. Agron. Crop Sci. 201 (5), 368–378. https://doi.org/10.1111/jac.12132.

Al-Wabel, M.I., Hussain, Q., Usman, A.R.A., Ahmad, M., Abduljabbar, A., Sallam, Abdulazeam, S., Ok, Y.S., 2017. Impact of biochar properties on soil conditions and agricultural sustainability: a review. Land Degrad. Dev. https://doi.org/10.1002/ldr.2829 n/a-n/a.

Ambaye, T.G., Vaccari, M., van Hullebusch, E.D., Amrane, A., Rtimi, S., 2020. Mechanisms and adsorption capacities of biochar for the removal of organic and inorganic pollutants from industrial wastewater. Int. J. Environ. Sci. Technol. https://doi.org/10.1007/s13762-020-03060-w.

Amini, S., Ghadiri, H., Chen, C., Marschner, P., 2016. Salt-affected soils, reclamation, carbon dynamics, and biochar: a review. J. Soils Sediments 16 (3), 939–953. https://doi.org/10.1007/s11368-015-1293-1.

Astuti, N., Wibowo, N., Ayub, M.R.S.S.N., 2018. The porosity calculation of various types of paper using Image analysis. Jurnal Pendidikan Fisika Indonesia 14, 46–51. https://doi.org/10.15294/jpfi.v14i1.9878.

Awan, S., Ullman, J., Ansari, K., Cui, L., Aa, S., Ippolito, J., 2020. Biochars reduce irrigation water sodium adsorption ratio. Biochar 3. https://doi.org/10.1007/s42773-020-00073-z.

Ayawei, N., Ebelegi, A.N., Wankasi, D., 2017. Modelling and interpretation of adsorption isotherms. J. Chem. 2017, 11. https://doi.org/10.1155/2017/3039817.

Betts, A.R., Chen, N., Hamilton, J.G., Peak, D., 2013. Rates and mechanisms of Zn2+ adsorption on a meat and bonemeal biochar. Environ. Sci. Technol. 47 (24), 14350–14357. https://doi.org/10.1021/es4032198.

Bispo, M.D., Schneider, J.K., da Silva Oliveira, D., Tomasini, D., da Silva Maciel, G.P., Schena, T., Onorevoli, B., Bjerk, T.R., Jacques, R.A., Krause, L.C., Caramão, E.B., 2018. Production of activated biochar from coconut fiber for the removal of organic compounds from phenolic. J. Environ. Chem. Eng. 6 (2), 2743–2750. https://doi.org/10.1016/j.jece.2018.04.029.

Carter, M.R., Gregorich, E.G., 2008. Soil Sampling and Methods of Analysis, second ed. CRC Press, Taylor & Francis Group, Boca Raton.

Chatterjee, R., Sajjadi, B., Chen, W.-Y., Mattern, D., Hammer, N., Raman, V., Dorris, A., 2020. Effect of pyrolysis temperature on physicochemical properties and acoustic-based amination of biochar for efficient CO2 adsorption. Front. Energy Res. 8, 85. https://doi.org/10.3389/fenrg.2020.00085.

Chen, T., Zhang, Y., Wang, H., Lu, W., Zhou, Z., Zhang, Y., Ren, L., 2014. Influence of pyrolysis temperature on characteristics and heavy metal adsorptive performance of biochar derived from municipal sewage sludge. Bioresour. Technol. 164C, 47–54. https://doi.org/10.1016/j.biortech.2014.04.048.

Chen, Z., Xiao, X., Chen, B., Zhu, L., 2015. Quantification of chemical states, dissociation constants and contents of oxygen-containing groups on the surface of biochars produced at different temperatures. Environ. Sci. Technol. 49 (1), 309–317. https://doi.org/10.1021/es5043468.

Cheng, W., Liu, C., Tong, T., Epsztein, R., Sun, M., Verduzco, R., Ma, J., Elimelech, M., 2018. Selective removal of divalent cations by polyelectrolyte multilayer nanofiltration membrane: role of polyelectrolyte charge, ion size, and ionic strength. J. Membr. Sci. 559 https://doi.org/10.1016/j.memsci.2018.04.052.

Daffalla, S., Mukhtar, H., Shaharun, M., 2020. Preparation and characterization of rice husk adsorbents for phenol removal from aqueous systems. PLoS One 15, e0243540. https://doi.org/10.1371/journal.pone.0243540.

Deliyanni, E., Arampatzidou, A., Tzoupanos, N., Matis, K., 2012. Adsorption of Pb^{2+} using mesoporous activated carbon and its effects on surface modifications. Adsorpt. Sci. Technol. 30, 627–646. https://doi.org/10.1260/0263-6174.30.7.627.

Dharmakeerthi, R.S., Chandrasiri, J.A.S., Edirimanne, V.U., 2012. Effect of rubber wood biochar on nutrition and growth of nursery plants of Hevea brasiliensis established in an Ultisol. SpringerPlus 1 (1). https://doi.org/10.1186/2193-1801-1-84, 84-84.

Do, P.T.M., Ueda, T., Kose, R., Nguyen, L.X., Okayama, T., Miyanishi, T., 2019. Properties and potential use of biochars from residues of two rice varieties, Japanese Koshihikari and Vietnamese IR50404. J. Mater. Cycles Waste Manag. 21 (1), 98–106. https://doi.org/10.1007/s10163-018-0768-8.

Dume, B., Yadessa, G., Tadesse, S., 2015. Characterization of biochar produced at different temperatures and its effect on acidic nitosol of Jimma, Southwest Ethiopia. Int. J. Soil Sci. 10, 63–73. https://doi.org/10.3923/ijss.2015.63.73.

Fathy, M., Mousa, M.A., Moghny, T.A., Awadallah, A.E., 2017. Characterization and evaluation of amorphous carbon thin film (ACTF) for sodium ion adsorption. Appl. Water Sci. 7 (8), 4427–4435. https://doi.org/10.1007/s13201-017-0588-3.

Fidel, R.B., Laird, D.A., Spokas, K.A., 2018. Sorption of ammonium and nitrate to biochars is electrostatic and pH-dependent. Sci. Rep. 8 (1), 17627. https://doi.org/10.1038/s41598-018-35534-w.

Gamage, D.N.V., Mapa, R.B., Dharmakeerthi, R.S., Biswas, A., 2016. Effect of rice-husk biochar on selected soil properties in tropical Alfisols. Soil Res. 54 (3), 302–310. https://doi.org/10.1071/SR15102.

Gunarathne, V., Senadeera, A., Gunarathne, U., Biswas, J.K., Almaroai, Y.A., Vithanage, M., 2020. Potential of biochar and organic amendments for reclamation of coastal acidic-salt affected soil. Biochar 2 (1), 107–120. https://doi.org/10.1007/s42773-020-00036-4.

Guo, X., Li, M., Liu, A., Jiang, M., Niu, X., Liu, X., 2020. Adsorption mechanisms and characteristics of Hg2+ removal by different fractions of biochar. Water 12, 2105. https://doi.org/10.3390/w12082105.

Haris, M., Hamid, Y., Usman, M., Wang, L., Saleem, A., Su, F., Guo, J., Li, Y., 2021. Crop-residues derived biochar: synthesis, properties, characterization and application for the removal of trace elements in soils. J. Hazard Mater. 416, 126212. https://doi.org/10.1016/j.jhazmat.2021.126212.

Hassan, M., Liu, Y., Naidu, R., Parikh, S.J., Du, J., Qi, F., Willett, I.R., 2020. Influences of feedstock sources and pyrolysis temperature on the properties of biochar and functionality as adsorbents: a meta-analysis. Sci. Total Environ. 744, 140714. https://doi.org/10.1016/j.scitotenv.2020.140714.

Hettiarachchi, E., Perera, R., Perera, C., Kottegoda, N., 2015. Activated coconut coir for removal of sodium and magnesium ions from saline water. Desalination Water Treat. 1–12. https://doi.org/10.1080/19443994.2015.1129649.

Isaac, O.A., Olufemi, A.A., 2020. In: Saleh, Hosam M. (Ed.), Agricultural Solid Wastes: Causes, Effects, and Effective Management, Strategies of Sustainable Solid Waste Management. IntechOpen. https://doi.org/10.5772/intechopen.93601. Available from: https://www.intechopen.com/chapters/73517.

Kaur, P., Kaur, P., Kaur, K., 2020. Adsorptive removal of imazethapyr and imazamox from aqueous solution using modified rice husk. J. Clean. Prod. 244, 118699. https://doi.org/10.1016/j.jclepro.2019.118699.

Kaur, V., Sharma, P., 2020. Application of biochar as an adsorbent and its significance on berseem (Trifolium alexandrinum) growth parameters in farm soil contaminated with PAH. J. Soil Sci. Plant Nutr. https://doi.org/10.1007/s42729-019-00167-z.

Leng, L., Xiong, Q., Yang, L., Li, H., Zhou, Y., Zhang, W., Jiang, S., Li, H., Huang, H., 2021. An overview on engineering the surface area and porosity of biochar. Sci. Total Environ. 763, 144204. https://doi.org/10.1016/j.scitotenv.2020.144204.

Li, B., Liu, D., Lin, D., Xie, X., Wang, S., Xu, H., Wang, J., Huang, Y., Zhang, S., Hu, X., 2020. Changes in biochar functional groups and its reactivity after volatile–char interactions during biomass pyrolysis. Energy Fuels 34, 14291–14299. https://doi.org/10.1021/acs.energyfuels.0c03243.

Li, H., Dong, X., da Silva, E.B., de Oliveira, L.M., Chen, Y., Ma, L.Q., 2017. Mechanisms of metal sorption by biochars: biochar characteristics and modifications. Chemosphere 178, 466–478. https://doi.org/10.1016/j.chemosphere.2017.03.072.

Machado, R., Serralheiro, R., 2017. Soil salinity: effect on vegetable crop growth. management practices to prevent and mitigate soil salinization. Horticulturae 3, 13. https://doi.org/10.3390/horticulturae3020030.

Maliutina, K., Tahmasebi, A., Yu, J., 2018. Effects of pressure on morphology and structure of bio-char from pressurized entrained-flow pyrolysis of microalgae. Data Brief 18, 422–431. https://doi.org/10.1016/j.dib.2018.03.048.

Minhas, P.S., Ramos, T.B., Ben-Gal, A., Pereira, L.S., 2020. Coping with salinity in irrigated agriculture: crop evapotranspiration and water management issues. Agric. Water Manag. 227, 105832. https://doi.org/10.1016/j.agwat.2019.105832.

Mireles, S., Parsons, J., Trad, T., Cheng, C.L., Kang, J., 2019. Lead removal from aqueous solutions using biochars derived from corn stover, orange peel, and pistachio shell. Int. J. Environ. Sci. Technol. 16 (10), 5817–5826. https://doi.org/10.1007/s13762-018-02191-5.

Nan, Q., Xin, L., Qin, Y., Waqas, M., Wu, W., 2021. Exploring long-term effects of biochar on mitigating methane emissions from paddy soil: a review. Biochar 3 (2), 125–134. https://doi.org/10.1007/s42773-021-00096-0.

Nguyen, B.T., Le, L.B., Pham, L.P., Nguyen, H.T., Tran, T.D., Van Thai, N., 2021. The effects of biochar on the biomass yield of elephant grass (Pennisetum Purpureum Schumach) and properties of acidic soils. Ind. Crop. Prod. 161, 113224. https://doi.org/10.1016/j.indcrop.2020.113224.

Nguyen, B.T., Trinh, N.N., Le, C.M.T., Nguyen, T.T., Tran, T.V., Thai, B.V., Le, T.V., 2018. The interactive effects of biochar and cow manure on rice growth and selected properties of salt-affected soil. Arch. Agron Soil Sci. 64 (12), 1744–1758. https://doi.org/10.1080/03650340.2018.1455186.

Pham, T.T.H., Vu, X.H., Trang, T.T., Ca, N.X., Dien, N.D., Van Hai, P., Ha Lien, N.T., Trong Nghia, N., Kim Chi, T.T., 2021. Enhance Raman scattering for probe methylene blue molecules adsorbed on ZnO microstructures due to charge transfer processes. Opt. Mater. 120, 111460. https://doi.org/10.1016/j.optmat.2021.111460.

Richards, L.A. (Ed.), 1954. Diagnosis and Improvement of Saline Alkali Soils. USDA Handbook No. 60, Washington, DC, USA.

Rostamian, R., Heidarpour, M., Mousavi, S.-F., Majid, A., 2015. Characterization and sodium sorption capacity of biochar and activated carbon prepared from rice husk. J. Agric. Sci. Technol. 17, 1057–1069. https://jast.modares.ac.ir/article-23-3837-en.pdf.

Saeed, A., yub harun, N., Sufian, S., Bilad, M., Nufida, B., Ismail, N., Zakaria, Z., Jagaba, A.H., Ghaleb, A., Al-dhawi, B., 2021. Modeling and optimization of biochar based adsorbent derived from Kenaf using response surface methodology on adsorption of Cd2+. Water 13, 999. https://doi.org/10.3390/w13070999.

Sahab, S., Suhani, I., Srivastava, V., Chauhan, P.S., Singh, R.P., Prasad, V., 2021. Potential risk assessment of soil salinity to agroecosystem sustainability: current status and management strategies. Sci. Total Environ. 764, 144164. https://doi.org/10.1016/j.scitotenv.2020.144164.

Saifullah, Dahlawi, S., Naeem, A., Rengel, Z., Naidu, R., 2018. Biochar application for the remediation of salt-affected soils: challenges and opportunities. Sci. Total Environ. 625, 320–335. https://doi.org/10.1016/j.scitotenv.2017.12.257.

Sarkar, S., Skalicky, M., Hossain, A., Brestic, M., Saha, S., Garai, S., Ray, K., Brahmachari, K., 2020. Management of crop residues for improving input use efficiency and agricultural sustainability. Sustainability 12 (23), 9808. https://doi.org/10.3390/su12239808.

Schnepf, N.R., Manoj, C., Kuvshinov, A., Toh, H., Maus, S., 2014. Tidal signals in ocean-bottom magnetic measurements of the Northwestern Pacific: observation versus prediction. Geophys. J. Int. 198 (2), 1096–1110. https://doi.org/10.1093/gji/ggu190.

Shrivastava, P., Kumar, R., 2014. Soil salinity: a serious environmental issue and plant growth promoting bacteria as one of the tools for its alleviation. Saudi J. Biol. Sci. 22 https://doi.org/10.1016/j.sjbs.2014.12.001.

Sousa, D.V.d., Guimarães, L.M., Félix, J.F., Ker, J.C., Schaefer, C.E.R.G., Rodet, M.J., 2020. Dynamic of the structural alteration of biochar in ancient Anthrosol over a long timescale by Raman spectroscopy. PLoS One 15 (3), e0229447. https://doi.org/10.1371/journal.pone.0229447.

Taha, A.A., Ahmed, A.M., Abdel Rahman, H.H., Abouzeid, F.M., Abdel Maksoud, M.O., 2017. Removal of nickel ions by adsorption on nano-bentonite: equilibrium, kinetics, and thermodynamics. J. Dispersion Sci. Technol. 38 (5), 757–767. https://doi.org/10.1080/01932691.2016.1194211.

Tomczyk, A., Sokołowska, Z., Boguta, P., 2020. Biochar physicochemical properties: pyrolysis temperature and feedstock kind effects. Rev. Environ. Sci. Biotechnol. 19 (1), 191–215. https://doi.org/10.1007/s11157-020-09523-3.

Tripathi, N., Hills, C.D., Singh, R.S., Atkinson, C.J., 2019. Biomass waste utilisation in low-carbon products: harnessing a major potential resource. npj Climate and Atmospheric Science 2 (1), 35. https://doi.org/10.1038/s41612-019-0093-5.

Wang, S., Li, W., Yin, X., Wang, N., Yuan, S., Yan, T., Qu, S., Yang, X., Chen, D., 2019. Cd (II) ddsorption on different modified rice straws under FTIR spectroscopy as influenced by initial pH, Cd(II) concentration, and ionic strength. Int. J. Environ. Res. Publ. Health 16, 4129. https://doi.org/10.3390/ijerph16214129.

Wang, Y., Xiao, X., Chen, B., 2018. Biochar impacts on soil silicon dissolution kinetics and their interaction mechanisms. Sci. Rep. 8 https://doi.org/10.1038/s41598-018-26396-3.

Wu, Q., Xian, Y., He, Z., Zhang, Q., Yang, G., Zhang, X., Qi, H., Ma, J., Xiao, Y., Long, L., 2019. Adsorption characteristics of Pb(II) using biochar derived from spent mushroom substrate. Sci. Rep. 9 https://doi.org/10.1038/s41598-019-52554-2.

Xiong, J., Tian, Y., Wang, J., Liu, W., Chen, Q., 2017. Comparison of coconut coir, rockwool, and peat cultivations for tomato production: nutrient balance, plant growth and fruit guality. Front. Plant Sci. 8 (1327) https://doi.org/10.3389/fpls.2017.01327.

Zhang, J., Tan, Z., Huang, Q., 2021. Study on principles and mechanisms of new biochar passivation of cadmium in soil. Biochar 3 (2), 161–173. https://doi.org/10.1007/s42773-021-00088-0.

Zhang, P., Chen, Y.-P., Wang, W., Shen, Y., Guo, J.-S., 2016. Surface plasmon resonance for water pollutant detection and water process analysis. Trac. Trends Anal. Chem. 85, 153–165. https://doi.org/10.1016/j.trac.2016.09.003.